LANGMUIR

Article

pubs.acs.org/Langmuir

Evaporation of Sessile Droplets Laden with Particles and Insoluble Surfactants

George Karapetsas,*[,†] Kirti Chandra Sahu,[‡] and Omar K. Matar[§]

[†]Department of Chemical Engineering, University of Patras, Patras 26500, Greece

[‡]Department of Chemical Engineering, Indian Institute of Technology Hyderabad, Sangareddy 502 285, Telangana, India

[§]Department of Chemical Engineering, Imperial College London, London SW7 2AZ, U.K.

Supporting Information

ABSTRACT: We consider the flow dynamics of a thin evaporating droplet in the presence of an insoluble surfactant and noninteracting particles in the bulk. On the basis of lubrication theory, we derive a set of evolution equations for the film height, the interfacial surfactant, and bulk particle concentrations, taking into account the dependence of liquid viscosity on the local particle concentration. An important ingredient of our model is that it takes into account the fact that the surfactant adsorbed at the interface hinders evaporation. We perform a parametric study to investigate how the presence of surfactants affects the evaporation process as well as the flow dynamics with and without the presence of particles in the bulk. Our numerical calculations show that the droplet lifetime is affected significantly by the balance between the ability of the surfactant to enhance spreading, suppressing the effect of thermal Marangoni stresses-induced motion, and to hinder the evaporation flux through the reduction of the effective interfacial area of evaporation, which tend to accelerate and decelerate the evaporation process, respectively. For particle-laden droplets and in the case of dilute solutions, the droplet lifetime is found to be weakly dependent on the initial particle concentration. We also show that the particle deposition patterns are influenced strongly by the direct effect of the surfactant on the evaporative flux; in certain cases, the "coffee-stain" effect is enhanced significantly. A discussion of the delicate interplay between the effects of capillary pressure and solutal and thermal Marangoni stresses, which drive the liquid flow inside of the evaporating droplet giving rise to the observed results, is provided herein.

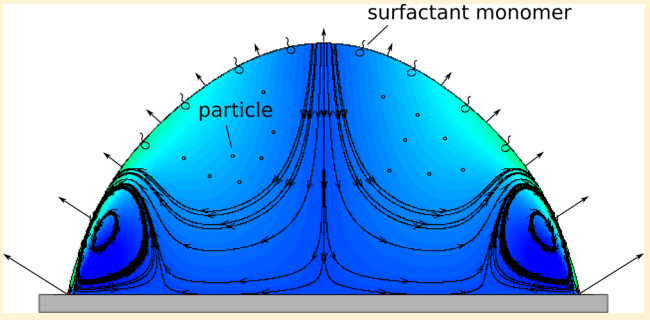

1. INTRODUCTION

Evaporation of droplets containing dispersed particles usually leads to an inhomogeneous residue with the most commonly observed pattern being a thin ring-shaped stain; this phenomenon is widely known as the coffee-stain or "coffee-ring" effect. Besides the pure scientific interest to understand the mechanisms responsible for this effect, it can also be important in a variety of technological applications. Evaporative particle deposition is involved in processes such as the controlled evaporative self-assembly (CESA),[1−4] fabrication of DNA/RNA microarrays,[5,6] or more traditional ones including for instance printing and coating.

The ability to control the deposition patterns depends strongly on our level of understanding of how the evaporation process takes place, and this has led many research groups to undertake experimental and theoretical work in this direction; informative reviews of these efforts can be found in refs 7−9. The first attempt to shed some light on the coffee-stain effect came from Deegan et al.[10−12] In these seminal studies, it was explained that when evaporation takes place with a pinned contact line, the ring is produced because of the radial capillary flow from the interior of the drop to the contact line to replenish the liquid that is lost by evaporation. As a result, the particles are carried toward the contact line and are being deposited there. However, as was noted later by Hu and Larson,[13−15] this is only a part of the story because the presence of thermal Marangoni flow may significantly alter the flow field inside of the droplet. In particular, it has been shown that in the absence of surfactants the presence of thermal gradients gives rise to a strong recirculating flow in the droplet, leading to particle deposition at the droplet center rather than the edge.[15]

Another factor that may affect the flow field is also the presence of any surfactants. In fact, the most common strategy in the literature to control the flow pattern inside an evaporating droplet is to utilize surface-active additives to induce Marangoni flows; other methods have also been suggested, for example, the use of electric fields.[16−19] Nevertheless, the mechanisms through which surfactants affect the evaporation process are not well understood and have been a topic of debate. It has been suggested that surfactants can be

Received: March 16, 2016
Revised: June 14, 2016
Published: June 14, 2016

DOI: 10.1021/acs.langmuir.6b01042
Langmuir 2016, 32, 6871−6881

responsible for suppressing the effect of thermal Marangoni flow by generating a counter gradient of surface tension, driving the liquid outward.[15,20] According to Hu and Larson,[15] given the well-known difficulty to keep water surfaces clear of contaminants, this could provide an explanation why in the case of evaporating water droplets, the net Marangoni flow was found to be rather weak.[10−12]

Recent experimental studies have shown that depending on the surfactant concentration or the type of surfactant it is possible to either enhance the coffee-stain effect or lead to a total flow inversion.[21−27] More specifically, Still et al.[22] achieved a uniform deposition of colloidal particles on glass by adding sodium dodecyl sulfate (SDS) to the drop dispersion. Sempels et al.[24] studied a bacterial system, that is, droplets of cultured *Pseudomonas aeruginosa*, and showed that the auto-production of surfactants suppresses the formation of a coffee ring. However, Crivoi and Duan[25,26] have shown that the formation of a coffee ring of graphite nanoparticles is enhanced with the addition of the cetyltrimethyl ammonium bromide (CTAB) surfactant. These authors underlined that the effect of the surfactant on the particle sticking probability can also be a decisive factor in the particle deposition pattern. Surfactants also affect the attachment strength of colloidal particles to the solid substrate, thus influencing particle deposition.[28] Very recently, Anyfantakis et al.[29] examined the surfactant-mediated interactions between particles and the liquid−gas and liquid−solid interfaces and found that these can also affect the final deposition pattern. The effect of electrostatic and van der Waals forces on the particle deposition process has been examined by Bhardwaj et al.[30] Finally, the coexistence of thermal and surfactant concentration gradients may give rise to fingering instabilities at the contact line, resulting in depositions with flowerlike patterns.[31]

To summarize, so far, it has been suggested that the presence of surfactants controls the following effects and phenomena: (a) Marangoni flow due to the presence of interfacial concentration gradients, (b) dynamics of the contact line, (c) particle−particle interactions, and (d) particle interactions with liquid−gas and liquid−solid interfaces. It is important to note, though, that besides these effects there is also another property of surfactants that has been largely ignored in the study of drying droplets. It is well known in the physical chemistry literature that surfactants may also inhibit the evaporation rate by reducing the effective area along the liquid−air interface through which evaporation is possible.[32−37] One question that arises is how this effect of surfactants on the evaporation flux may affect the flow dynamics and therefore the resulting particle deposition patterns.

The complexity and richness of dynamics due to the presence of coupled heat, mass and momentum transfer phenomena render the study of such systems quite challenging and, as was noted above, most studies so far have relied on experimental observations. In terms of theoretical modeling, people have considered either the case of nonvolatile droplets in the presence of surfactants[38−41] or evaporating droplets with particles and no surfactants.[42,43] The scope of this work is to investigate theoretically the case of a thin volatile droplet that contains an insoluble surfactant and noninteracting particles in the bulk.

To this end, we develop a lubrication model based on the so-called one-sided approximation[44−46] (assuming negligible vapor density, viscosity, and thermal conductivity), which allows us to concentrate solely on the liquid phase. Of course, it is anticipated that this approximation would not be able to provide quantitative predictions in cases where the evaporative process is diffusion limited, and therefore, the vapor phase is relevant. Nevertheless, this approach has proven to be quite useful in the qualitative description of various phenomena, for example, the prediction of the emergence of hydrothermal waves in evaporating droplets.[47] When quantitative predictions are needed, the two-sided approach proposed by Sultan et al.[48] can be more relevant, at the expense of increased complexity of the model. To account for the presence of particles, we employ a simple model applicable to dilute solutions, which was developed by Warner et al.[49] for studying evaporating films containing nanoparticles. Finally, we fully account for the presence of insoluble surfactant monomers at the liquid−gas interface. Crucially, our model takes into account the inhibiting effect of the monomers on the evaporative flux, which has been ignored by previous studies in the literature, and thus, it is possible to investigate how the droplet dynamics and resulting flow field can be affected by the balance between the ability of the surfactant to enhance spreading and to hinder the evaporation flux through the reduction of the effective interfacial area of evaporation.

The remainder of the paper is organized as follows. In section 2, we describe the system of governing equations and outline the numerical scheme that is used for the simulations. The results are presented and discussed in section 3. Finally, concluding remarks are given in section 4.

2. PROBLEM FORMULATION

We study the behavior of a droplet undergoing evaporation. The drop is laden with small particles and with an insoluble, nonvolatile surfactant, which adsorbs at the liquid−air interface. The fluid is considered to be Newtonian, with constant density ρ, specific heat capacity C_p, thermal conductivity λ, and viscosity, μ, which depends on particle concentration. The surface tension, σ, depends on the interfacial concentration of the surfactant, Γ, and local temperature, T; the particles are assumed to be surface-inactive. The drop is placed on a horizontal solid substrate and bounded from above using an inviscid gas (see Figure 1). We assume that, initially, the drop

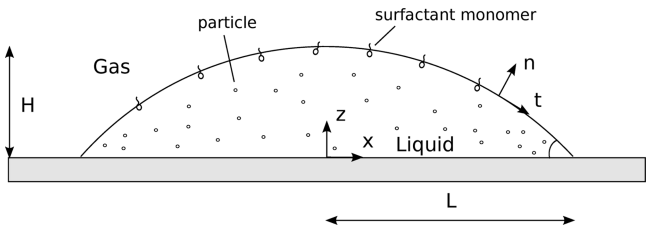

Figure 1. Schematic representation of an evaporating droplet resting on a solid surface of temperature T_w.

has maximal thickness H and half-width L. In the present work, we consider the drop to be very thin, and therefore, L is assumed to greatly exceed H so that the drop aspect ratio, $\varepsilon = H/L$, is assumed to be very small. The latter assumption permits the use of lubrication theory, which will be employed below to derive a set of evolution equations that govern the spreading process.

We use a Cartesian coordinate system, (x,z), to model the dynamics and the velocity field, $\mathbf{u} = (u,w)$ where u and w correspond to the horizontal and vertical components of the velocity field, respectively. The liquid−gas interface is located at

DOI: 10.1021/acs.langmuir.6b01042
Langmuir 2016, 32, 6871−6881

$z = h(x,t)$, whereas the liquid−solid and the solid−gas interfaces are located at $z = 0$.

The flow is incompressible and governed by the momentum, mass, and energy conservation equations given below

$$\rho(\mathbf{u}_t + \mathbf{u}\cdot\nabla\mathbf{u}) = \nabla\cdot\boldsymbol{\tau} \tag{1}$$

$$\nabla\cdot\mathbf{u} = 0 \tag{2}$$

$$\rho C_p(T_t + \mathbf{u}\cdot\nabla T) = \lambda\nabla^2 T \tag{3}$$

where τ is the total stress tensor,

$$\boldsymbol{\tau} = -p\mathbf{I} + \mu(\nabla\mathbf{u} + \nabla\mathbf{u}^T) \tag{4}$$

p is the pressure, and T is the temperature; ∇ and $\mathbf{I}$ denote the gradient operator and identity tensor, respectively. Unless stated otherwise, the subscripts denote partial differentiation with respect to x, z and time t.

Along the free surface ($z = h(x,t)$), it is necessary to distinguish between the liquid velocity $\mathbf{u}$ and the velocity of the interface $\mathbf{u}_s = (u_s,w_s)$. If J denotes the evaporative flux, $\mathbf{n} = (-h_x,1)/(1 + h_x^2)^{1/2}$ is the outward unit normal on the interface then

$$\mathbf{u} = \mathbf{u}_s + J/\rho\mathbf{n} \tag{5}$$

whereas the tangential components of both velocities, $\mathbf{u}_\tau = \mathbf{u} - (\mathbf{u}\cdot\mathbf{n})\mathbf{n} = \mathbf{u}_s - (\mathbf{u}_s\cdot\mathbf{n})\mathbf{n}$, are the same. Moreover, at $z = h(x,t)$, the velocity field satisfies the local mass, force, and energy balance in the liquid and gas phases[42,47]

$$\rho(\mathbf{u} - \mathbf{u}_s)\cdot\mathbf{n} = \rho_g(\mathbf{u}_g - \mathbf{u}_s)\cdot\mathbf{n} \tag{6}$$

$$J(\mathbf{u} - \mathbf{u}_g)\cdot\mathbf{n} - \mathbf{n}\cdot(\boldsymbol{\tau} - \boldsymbol{\tau}_g)\cdot\mathbf{n} = 2\kappa\sigma - \Pi \tag{7}$$

$$J(\mathbf{u} - \mathbf{u}_g)\cdot\mathbf{t} - \mathbf{n}\cdot(\boldsymbol{\tau} - \boldsymbol{\tau}_g)\cdot\mathbf{t} = -\nabla_s\sigma\cdot\mathbf{t} \tag{8}$$

$$J\left(L_v + \frac{1}{2}((\mathbf{u}_g - \mathbf{u}_s)\cdot\mathbf{n})^2 - \frac{1}{2}((\mathbf{u} - \mathbf{u}_s)\cdot\mathbf{n})^2\right) + \lambda\nabla T\cdot\mathbf{n} - \lambda_g\nabla T_g\cdot\mathbf{n} + (\boldsymbol{\tau}\cdot\mathbf{n})\cdot(\mathbf{u} - \mathbf{u}_s) - (\boldsymbol{\tau}_g\cdot\mathbf{n})\cdot(\mathbf{u}_g - \mathbf{u}_s) = 0 \tag{9}$$

Here, ρ_g, λ_g, $\mathbf{u}_g$, and T_g denote the density, thermal conductivity, velocity field, and temperature in the gas phase, respectively; L_v is the specific internal latent heat of vaporization.[50] $\mathbf{t} = (1,h_x)/(1+h_x^2)^{1/2}$ denotes the unit tangential vectors on the interface. 2κ is the mean curvature of the free surface, and ∇_s is the surface gradient operator, respectively, defined as

$$2\kappa = \nabla_s\cdot\mathbf{n} \qquad \nabla_s = (I - \mathbf{nn})\cdot\nabla \tag{10}$$

Π denotes the disjoining pressure, which accounts for the van der Waals interactions, defined as

$$\Pi = \frac{A}{6\pi h^3} \tag{11}$$

where A is the Hamaker constant.

Along the moving interface ($z = h(x,t)$), we also impose the kinematic boundary condition

$$h_t + u_s h_x = w_s \tag{12}$$

At the liquid−solid interface ($z = 0$), we set

$$u = 0 \qquad w = 0 \qquad T = T_w \tag{13}$$

2.1. Surfactant and Particle Transport. We consider that the droplet contains small particles with an initially uniform concentration, c_i. The concentration of particles in the bulk, c, is governed by an advection−diffusion equation

$$c_t + \mathbf{u}\cdot\nabla c = D_c\nabla^2 c \tag{14}$$

subject to the following boundary conditions

$$(\mathbf{n}\cdot\nabla c)_{z=0} = 0 \tag{15}$$

$$D_c(\mathbf{n}\cdot\nabla c)_{z=h} = c(\mathbf{u} - \mathbf{u}_s)\cdot\mathbf{n} \tag{16}$$

The viscosity of the fluid, $\mu(c)$, is assumed to be dependent locally on the concentration of particles in the bulk, c, through the following constitutive relation[51,52]

$$\mu(c) = \mu_c\left(1 - \frac{c}{c_\infty}\right)^{-2} \tag{17}$$

Here, c_∞ represents the maximum packing of the bulk particles; the magnitude of this parameter is determined by factors such as the particle size, shape, and packing configuration. A restriction of the present model is that it is applicable to dilute solutions. It should be noted though that as the droplet dries out the concentration of particles will increase and eventually become so high that this assumption will no longer hold. To properly account for this transition, a more complex model would be needed, for example, see Kaplan and Mahadevan.[43,53]

The behavior of the surfactant monomers is modeled by the following advection−diffusion equation

$$\Gamma_t - h_t(\mathbf{e}_z\cdot\nabla_s\Gamma) + \nabla_s\cdot(\mathbf{u}_\tau\Gamma) + (\nabla_s\cdot\mathbf{n})(\mathbf{u}_s\cdot\mathbf{n})\Gamma = D_\Gamma\nabla_s^2\Gamma \tag{18}$$

where D_Γ denotes the diffusion coefficient of the monomers at the liquid−air interface. As explained in refs 37, 54, and 55, the first two terms on the left-hand side together describe the temporal change of Γ along the normal to the moving interface, the third term accounts for the advection of the surfactant because of the liquid flow along the interface, and the fourth term accounts for the variation in surfactant concentration resulting from local changes in the interfacial area. Note that the total mass of the surfactant, M_{surf}, and particles, M_{par}, present in the liquid drop is conserved quantities, given by

$$\int_0^L \Gamma\,dx = M_{surf}$$

$$\int_0^L\int_0^h c\,dz\,dx = M_{par} \tag{19}$$

2.2. Constitutive Equations for Surface Tension and Evaporative Flux. To complete the description, a constitutive equation that describes the dependence of the interfacial tension on the surfactant concentration and interfacial temperature is required. To this end, we employ the following constitutive equation

$$\sigma = \sigma_c\left(1 + \frac{\Gamma}{\Gamma_\infty}\left[\left(\frac{\sigma_c}{\sigma_m}\right)^{1/3} - 1\right]\right)^{-3} + \left.\frac{\partial\sigma}{\partial T}\right|_{\Gamma=0}(T - T_{sat}) \tag{20}$$

which is based on the Sheludko equation of state[56,57] and assumes a linear dependence on the temperature. Here, σ_c and

DOI: 10.1021/acs.langmuir.6b01042
Langmuir 2016, 32, 6871−6881

σ_m are the surface tensions at $T = T_{sat}$ of a surfactant-free fluid and of maximal surfactant concentration, respectively.

Finally, we use the following nonequilibrium interfacial condition to model evaporative effects[45,46,58]

$$\frac{p_{ve}}{p_v} - 1 = \frac{p - p_v}{\rho R_g T_{sat}} + \frac{L_v}{R_g T_{sat}}\left(\frac{T|_h}{T_{sat}} - 1\right) \tag{21}$$

where p_{ve} is the equilibrium vapor pressure, $T|_h$ is the interfacial temperature, and R_g denotes the specific gas constant. The following equilibrium relation is also used for the evaporative flux, J[58]

$$J = \rho_v\left(\frac{R_g T_{sat}}{2\pi}\right)^{1/2}\left(\alpha_v\frac{p_{ve}}{p_v} - \beta_v\right) \tag{22}$$

In this expression, α_v and β_v are accommodation coefficients for evaporation and condensation, respectively. Near equilibrium, we note that α_v and β_v will be nearly equal. The surfactant adsorbed at the surface hinders the evaporation, and to account for this effect, we assume the following dependence on the interfacial surfactant concentration

$$\alpha_v(\Gamma) = \beta_v(\Gamma) = \frac{\Gamma_\infty}{\Gamma_\infty + \psi\Gamma} \tag{23}$$

where $\psi > 0$. At maximum packing, the accomodation coefficient becomes equal to $1/(1 + \psi)$ and this limit may be used for an estimation of ψ from experimental data. A typical range for the accommodation coefficients is between 0.001 and 1, which implies that $0 < \psi < 10^3$. In what follows, the effect of ψ on evaporation will be studied.

2.3. Scaling. The governing equations and boundary conditions are made dimensionless using the following scalings (tildes denote dimensionless variables)

$$(x, z, h) = L(\tilde{x}, \varepsilon\tilde{z}, \varepsilon\tilde{h}) \qquad t = \frac{L}{U}\tilde{t} \qquad (u, w) = U(\tilde{u}, \varepsilon\tilde{w})$$

$$(p, \Pi) = \frac{\mu_c UL}{H^2}(\tilde{p}, \tilde{\Pi}) \qquad T = \tilde{T}(T_w - T_{sat}) + T_{sat} \qquad \sigma = \tilde{\sigma}\sigma_c$$

$$J = \tilde{J}\frac{\lambda(T_w - T_{sat})}{HL_v} \qquad \Gamma = \tilde{\Gamma}\Gamma_\infty \qquad c = \tilde{c}c_i$$

$$M_{surf} = \tilde{M}_{surf}L\Gamma_\infty \qquad M_{par} = \tilde{M}_{par}LHc_i \tag{24}$$

where $U = \varepsilon\sigma_c/\mu_c$ is a characteristic velocity. The tildes are henceforth suppressed. The substitution of these scalings into the governing equations and boundary conditions, using the lubrication approximation ($\varepsilon \ll 1$), yields

$$u_x + w_z = 0 \tag{25}$$

$$p_x = (\mu u_z)_z \qquad p_z = 0 \tag{26}$$

$$T_{zz} = 0 \tag{27}$$

$$c_t + uc_x + wc_z = \frac{1}{Pe_c}\left(c_{xx} + \frac{c_{zz}}{\varepsilon^2}\right) \tag{28}$$

and

$$\Gamma_t + (u\Gamma)_x = \frac{\Gamma_{xx}}{Pe_\Gamma} \quad \text{at } z = h \tag{29}$$

The dimensionless viscosity is given by

$$\mu = (1 - \chi c)^{-2} \tag{30}$$

where $\chi = c_i/c_\infty$. The dimensionless groups $Pe_i = UL/D_i$ ($i = \Gamma, c$) are Peclet numbers representing a ratio of convective to diffusive time scales for the monomers at the free surface and the particles in the bulk, respectively.

The solution of the above equations are obtained subject to the following boundary conditions at the solid wall ($z = 0$)

$$u = 0 \qquad w = 0 \qquad T = 1 \tag{31}$$

Along the liquid−gas interface, $z = h(x,t)$, the boundary conditions become

$$h_t + uh_x - w + EJ = 0$$

$$u_z = \frac{\sigma_x}{\mu}$$

$$p = p_v + \mathcal{R}J^2 - \varepsilon^2\sigma h_{xx} - \frac{\mathcal{A}}{h^3}$$

$$J\left(1 + \frac{E^2}{2\mathcal{L}D}J^2\right) + T_z = 0 \tag{32}$$

where $E = \lambda(T_w - T_{sat})/(\varepsilon U\rho HL_v)$ is the evaporation number, $\mathcal{A} = A/(6\pi HL\mu U)$ is the dimensionless Hamaker constant, $\mathcal{R} = \varepsilon\lambda^2(T_w - T_{sat})^2/(L_v{}^2\rho_g\mu_c UH)$ is the vapor recoil number, $\mathcal{L} = \varepsilon^2 L_v/U^2$, and $D = \varepsilon^{-2}\rho_g/\rho$. Here, we have adopted the one-sided model[44] assuming that $(\rho_g/\rho, \mu_g/\mu_c, \lambda_g/\lambda) \ll 1$. The typical values of the physical properties are given in Table 1

Table 1. Order of Magnitude Estimates of the Physical Constants and a Typical Range of the Dimensionless Parameters

constants	typical values	parameter	typical range
L (m)	10^{-3}	ε	0.005−0.2
μ_c (Pa s)	10^{-3}	E	0−0.001
ρ (kg/m^3)	10^3	K	10^{-5}−0.1
λ (W/mK)	0.5	D	0.1−10^2
μ_g (Pa s)	10^{-5}	Σ	1−5
ρ_g (kg/m^3)	1	ψ	0−10^3
λ_g (W/mK)	0.02	χ	0.01−0.1
σ_c (N/m)	0.07	Pe_Γ	10^2 to 10^6
L_v (J/kg)	10^6	Pe_c	10−10^5
A (J)	10^{-19}	$\mathcal{R}$	10^{-4}−0.1
		$\mathcal{L}$	1−10^3
		$\mathcal{A}$	10^{-5} to 10^{-9}
		Δ	10^{-3} to 10^{-7}

along with a typical range of all dimensionless parameters. As shown in Table 1, the parameters $\mathcal{R}$ and $\mathcal{L}$ are typically small and the model may be further simplified by assuming that $\mathcal{R} \ll 1$ and $\mathcal{K} \ll 1$.

The constitutive equation for the evaporative flux is given by

$$(1 + \psi\Gamma)KJ = \Delta(p - p_v) + T|_h \tag{33}$$

where

$$\Delta = \frac{\mu_c UL T_{sat}}{\rho H^2 L_v(T_w - T_{sat})} \qquad K = \frac{\lambda(2\pi R_g T_{sat}{}^3)^{1/2}}{\rho_g HL_v{}^2} \tag{34}$$

By solving eqs 25−27 subject to boundary conditions (eqs 31 and 32) and adopting the rapid vertical diffusion approximation

DOI: 10.1021/acs.langmuir.6b01042
Langmuir 2016, 32, 6871−6881

for the bulk concentrations,[41,59] we can derive the following equations

$$h_t = \left(\frac{h^3}{3\mu}p_x - \sigma_x\frac{h^2}{2\mu}\right)_x - EJ \tag{35}$$

$$T = 1 - Jz \tag{36}$$

$$\Gamma_t + (u\Gamma)_x = \frac{\Gamma_{xx}}{Pe_\Gamma} \tag{37}$$

$$c_t + \bar{u}c_x = \frac{1}{Pe_c}\frac{(hc_x)_x}{h} + \frac{EJc}{h} \tag{38}$$

where the pressure gradient and average streamwise velocity component are, respectively, given by

$$p_x = -\varepsilon^2(\sigma h_{xx})_x - \Pi_x \tag{39}$$

$$\bar{u} = -\frac{h^2}{3\mu}p_x + \sigma_x\frac{h}{2\mu} \tag{40}$$

we have retained capillary contributions despite the fact that they arise to order $O(\varepsilon^2)$ in our model because we expect them to provide non-negligible contributions in highly curved regions in the flow.[60] Here, Π denotes the dimensionless disjoining pressure, $\Pi = \mathcal{A}/h^3$. In the above equations, the evaporative flux, J, is evaluated using the following expression

$$J = \frac{-\Delta[\varepsilon^2([1+\Gamma(\Sigma^{1/3}-1)]^{-3} - \gamma)h_{xx} + \mathcal{A}/h^3] + 1}{(1+\psi\Gamma)K + h(\Delta\varepsilon^2\gamma h_{xx} + 1)} \tag{41}$$

the dimensionless form of the equation of state for the liquid−gas surface tension is given by

$$\sigma = [1 + \Gamma(\Sigma^{1/3} - 1)^{-3}] - \gamma T \tag{42}$$

where $\Sigma = \sigma_c/\sigma_m$ and $\gamma = -\partial\sigma/\partial T|_{\Gamma=0}(T_w - T_{sat})/\sigma_c$. We note that the effect of surfactants on J enters through the parameter ψ (and also through the dependence of σ on Γ in the capillary contribution to the pressure).

It is useful to note that the bulk average velocity, $\bar{u}$, given by eq 40 can be also decomposed as follows

$$\bar{u} = \bar{u}_{ca} + \bar{u}_{cg} + \bar{u}_{tg} \tag{43}$$

where each contribution is expressed by

$$\bar{u}_{ca} = -\frac{h^2}{3\mu}p_x \qquad \bar{u}_{cg} = -\frac{3\Gamma_x(\Sigma^{1/3}-1)}{[1+\Gamma(\Sigma^{1/3}-1)]^4}\frac{h}{2\mu}$$

$$\bar{u}_{tg} = -\gamma T_x\frac{h}{2\mu} \tag{44}$$

Each of the three different components corresponds to a different mechanism that acts to drive the liquid inside of the evaporating droplet. Here, $\bar{u}_{ca}$ denotes the velocity that is caused by the presence of the capillary effects, whereas $\bar{u}_{cg}$ and $\bar{u}_{tg}$ correspond to the effect of Marangoni stresses. More specifically, $\bar{u}_{cg}$ denotes the velocity due to the presence of surfactant concentration gradients, whereas $\bar{u}_{tg}$ denotes the velocity due to the thermal gradients along the interface.

2.4. Initial and Boundary Conditions. Solutions are obtained starting from the following initial conditions for h, T, c, and Γ, which correspond to a droplet with constant curvature at rest with uniform temperature and all species in equilibrium.

$$h(x, t=0) = \max[h_\infty, 1 - x^2]$$

$$(\Gamma, c)(x, t=0) = 0.5(1 + \tanh[100(1-x)])$$

$$T(x, t=0) = 1 \tag{45}$$

In addition, we assume that the droplet is released onto an ultrathin film of uniform thickness

$$h_\infty = (\mathcal{A}\Delta)^{1/3} \tag{46}$$

This film is adsorbed from the atmosphere, and it is stabilized by van der Waals forces. The presence of this film, which is stabilized because of the fact that evaporation becomes suppressed by the action of attractive van der Waals forces, helps alleviate the stress singularity that could arise at the moving contact line. Regarding the boundary conditions in the x direction, we impose the following

$$h_x(0,t) = h_{xxx}(0,t) = h_x(x_\infty,t) = h_{xxx}(x_\infty,t) = 0$$

$$(\Gamma_x, c_x)(0,t) = (\Gamma_x, c_x)(x_\infty,t) = 0 \tag{47}$$

3. RESULTS AND DISCUSSION

The evaporation of a surfactant-laden liquid drop with particles is a parametrically rich problem. We begin our study by examining the flow in the case of an insoluble surfactant without particles and proceed with simulations in the presence of a finite particle concentration to examine the effect of various system parameters on the resulting particle deposition. Numerical solutions were obtained over a wide range of parameter values. The "base" case, however, is characterized by parameter values that are broadly typical of experimental settings: $\varepsilon = 0.1$, $K = 0.1$, $\Sigma = 5$, $\mathcal{A} = 10^{-6}$, $\Delta = 10^{-3}$, $Pe_\Gamma = 10^3$, and $Pe_c = 10$; these values will be kept constant unless otherwise noted. In the parametric study that will be presented below, we will vary the parameters M_{surf}, ψ, γ, E, M_{par}, and χ. According to eq 46 for the given set of parameters, the height of the precursor film used is $h_\infty = 10^{-3}$.

3.1. Surfactant-Laden Droplets without Particles. *3.1.1. $\psi = 0$.* We begin our study by examining first the evaporation process of a particle-free droplet. For the moment, we will not take into account the effect of the surfactant on the evaporative flux and neglect the primary dependence of J on Γ by setting $\psi = 0$; we note that J remains dependent on Γ through the capillary pressure term in the numerator of eq 41. In Figure 2a,b, we show the spatiotemporal variation of the drop height, for the particle-free case, in the presence and absence of the surfactant, respectively. In the surfactant-free case, the droplet dewets the surface during all stages of the evaporation process as is evident from Figure 2c, which demonstrates that the contact line location, x_c, undergoes a monotonic decrease with time. This decrease is retarded during the intermediate stages of droplet evaporation, which can be attributed to the fact that near the contact line region the capillary flow becomes stronger drawing more liquid toward the contact line in contrast to the surfactant-laden case; this is demonstrated in Figure 3a,b where we plot the profile of $\bar{u}_{ca}$, that is, the velocity component, which is due to the capillary pressure. The presence of thermal gradients gives rise to thermal Marangoni stresses, which drive liquid toward the droplet center, thus leading to the increase of the interfacial height at the droplet apex during an intermediate stage of the

DOI: 10.1021/acs.langmuir.6b01042
Langmuir 2016, 32, 6871−6881

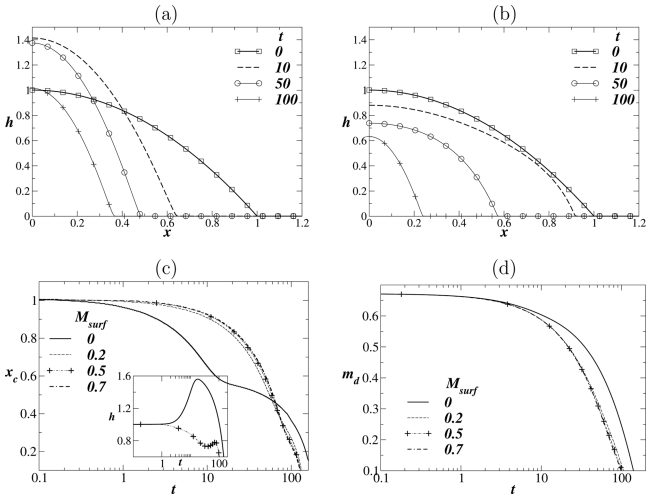

Figure 2. Evolution of the drop profile for (a) $M_{surf} = 0$ and (b) $M_{surf} = 0.5$. Evolution of the (c) position of the contact line and (d) mass of the drop for different values of M_{surf}. The rest of the parameter values are $E = 0.005$, $M_{par} = 0$, $\psi = 0$, $\chi = 0$, and $\gamma = 0.1$. The inset to panel (c) also shows the temporal evolution of the maximal film thickness, h_{max}, for $M_{surf} = 0$ and $M_{surf} = 0.5$ shown by solid and dashed lines, respectively.

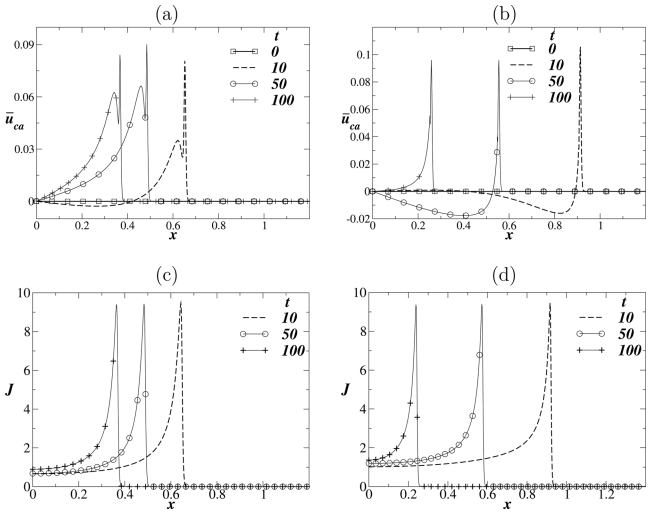

Figure 3. Profiles of $\bar{u}_{ca}$ at different time instants for (a) $M_{surf} = 0$ and (b) $M_{surf} = 0.5$. Profiles of the evaporative flux, J, at different time instants for (c) $M_{surf} = 0$ and (d) $M_{surf} = 0.5$. The rest of the parameter values are $E = 0.005$, $M_{surf} = 0$, $\psi = 0$, $\chi = 0$, and $\gamma = 0.1$.

dynamics before decreasing monotonically with time; this is also depicted clearly in the inset of Figure 2c. An animation of the droplet profile along with the velocity field (x component) and the streamlines is given in the Supporting Information (Movies S1 and S2). Snapshots at two time instants ($t = 10$ and 50) are depicted in Figure 4 for (a–c) $M_{surf} = 0$ (see Movie S1) and (d–f) $M_{surf} = 0.5$ (see Movie S2); c and f depict a zoom near the contact line at $t = 50$. Here, it is shown clearly that the thermal Marangoni stresses give rise to a recirculation vortex, which grows significantly until it engulfs the whole droplet; the direction of the vortex is in agreement with previous studies for substrates of infinite conductivity.[13,15,61] The action of thermal Marangoni stresses is also responsible for the enhancement of the dewetting process.

In the presence of the surfactant, the droplet does not retract during the early stages of the evaporation process. In fact, the contact line position remains essentially pinned up to $O(1)$ timescales before receding. As shown in Figure 2b,c, the dewetting process is not accompanied by an increase in the droplet thickness at the flow origin (see the inset of Figure 2c), and although there appears to be a retardation of the contact line recession during the latest stages of evaporation, it is much less significant than that of the surfactant-free case. A more detailed look at the flow field (see Figure 4d–f) reveals a drastic change due to the effect of surfactants. At early times, a counter-rotating vortex arises in the contact line region, which grows and eventually takes over; a stagnation point also arises in the contact line region (see Figure 4f). These results are in line with experimental observations.[22,27] As will be shown below, this is merely because of the action of surfactant concentration gradients, which significantly reduce or even neutralize the effect of thermal Marangoni stresses. An inspection of the temporal variation of the droplet mass, m_d, shown in Figure 2d, also reveals that the presence of the surfactant accelerates the evaporation process, though one should note again that the effect of the surfactant on the evaporative flux has been largely neglected in generating these results by setting $\psi = 0$ (though the Γ contribution to the capillary pressure in J [see eq 41] remains).

In Figure 3c,d, we show the development of the evaporative flux, J, for the surfactant-free and surfactant-laden cases, and the same parameters are used to generate Figure 2. For the results shown in this figure, for which $\psi = 0$, it appears that the surfactant makes little difference to the overall structure of J and its maximal value. The latter observation is a clear indication that the acceleration of droplet evaporation should actually be attributed to the fact that the droplet remains flatter for longer times, which leads to an increase of the effective interfacial area of evaporation. As is depicted in Figure 3c,d, the evaporative flux is highly localized in the contact line region, where it can be approximated by

$$J \sim \frac{1 - \Delta\Pi}{(1 + \psi\Gamma)K} \tag{48}$$

The flux exhibits a long decay "tail" toward the droplet apex where its value is given by the following approximate formula

$$J \sim \frac{1}{h + (1 + \psi\Gamma)K} \tag{49}$$

In the $\psi = 0$ case, eqs 48 and 49 reduce to $J \sim (1 - \Delta\Pi)/K$ and $J \sim 1/(h + K)$, respectively.

The location of the evaporative flux in relation to the contact line is shown more clearly in Figure 5 for the surfactant-laden case ($M_{surf} = 0.5$) at $t = 1$ and $t = 10$ during the dynamics in panels (a) and (b), with enlarged versions of the contact line region depicted in panels (c) and (d), respectively. Also shown in this figure are the corresponding profiles for the interfacial surfactant concentration, Γ, and the streamwise component of the interfacial velocity, $u(z = h)$. It is seen that Γ remains approximately constant over a large proportion of the drop before undergoing a rapid decrease as the contact line region is approached. The concentration Γ then exhibits a sharp increase to a maximal value (indicated by the arrows in panels c and d) located immediately downstream of the contact line and the location of the maximal value of J; this is followed by a decay to zero in the precursor film region. The spatial profile of Γ is

DOI: 10.1021/acs.langmuir.6b01042
Langmuir 2016, 32, 6871–6881

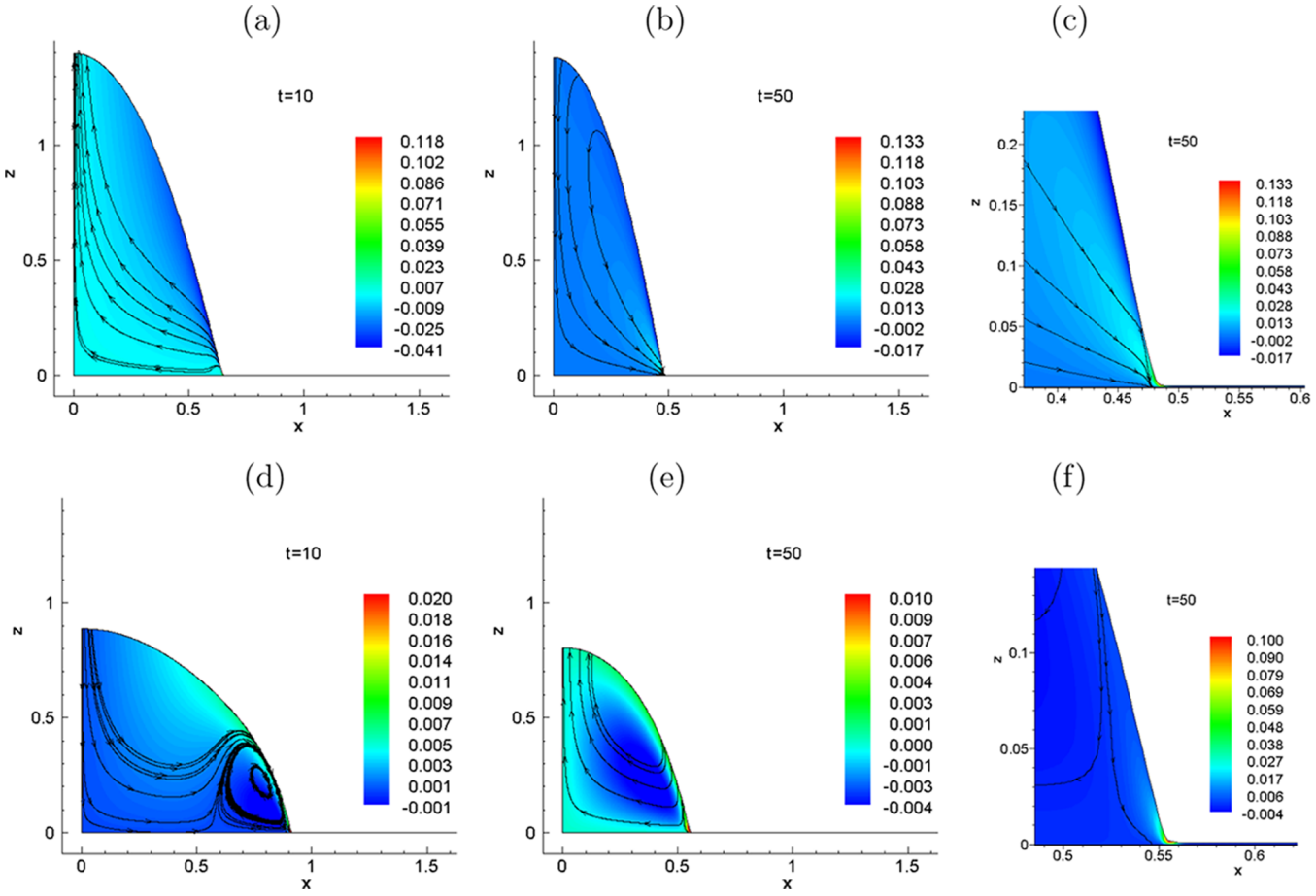

Figure 4. Contour plots of x velocity, u, along with streamlines for (a–c) $M_{surf} = 0$ and (d–f) $M_{surf} = 0.5$ at $t = 10$ and 50; c and f depict a zoom near the contact line at $t = 50$. The rest of the parameter values are $E = 0.005$, $M_{par} = 0$, $\psi = 0$, $\chi = 0$, and $\gamma = 0.1$. Animations of these simulations are available: (a–c) Movie S1 and (d–f) Movie S2 in the Supporting Information.

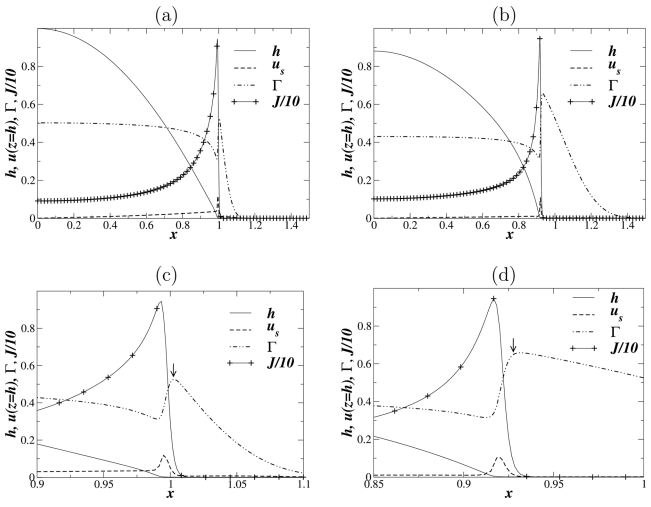

Figure 5. Profiles of the drop height, h, streamwise liquid velocity at the interface, $u(z = h)$, surfactant concentration, Γ, and evaporative flux, J, at (a) $t = 1$ and (b) $t = 10$. The corresponding zoomed views are presented in panels (c) and (d), respectively. The rest of the parameter values are $M_{surf} = 0.5$, $M_{par} = 0$, $\psi = 0$, $\chi = 0$, and $\gamma = 0.1$.

reminiscent of the profile seen in the case of surfactant-enhanced spreading in the absence of evaporation.[41] A major difference is that here we do not account for the explicit presence of a contact line as was reported in ref 41 but use instead a precursor model to relieve the contact line singularity.

Therefore, in our case, the surfactant is allowed to diffuse ahead of the contact line, which is responsible for the decay of Γ in that region; note that there is no flow present in the precursor film. Such behavior is not unreasonable and would actually be expected in the case of a prewetted solid surface; it could also resemble the case where the surfactant adsorbs at the solid substrate through the contact line and diffuses ahead of the drop.[41,59] It is also seen in Figure 4c,d that the interfacial liquid velocity $u(z = h)$ increases gradually within the drop because of the Marangoni contribution from $h\Gamma_x$ before undergoing rapid variation in the immediate vicinity of the contact line region where it exhibits a maximum because of the strong capillary flow there; beyond its maximal value, $u(z = h)$ decays rapidly to zero in the precursor film.

3.1.2. $\psi > 0$. Next, we examine the effect of the surfactant on evaporation by exploring the influence of the parameter ψ on the temporal evolution of the droplet mass. An inspection of Figure 6a reveals that an increase in ψ has an overall retarding effect on the evaporation process, leading to an increase in the droplet lifetime. This may also be expected by appealing to eq 48: it is clear from this expression that increasing ψ leads to a decrease in J, and this is responsible for the trends shown in Figure 6a. From this expression, we also deduce that increasing Γ leads to a decrease in the maximal value of J near the contact line. However, this is not reflected in the droplet lifetime, which

DOI: 10.1021/acs.langmuir.6b01042
Langmuir 2016, 32, 6871–6881

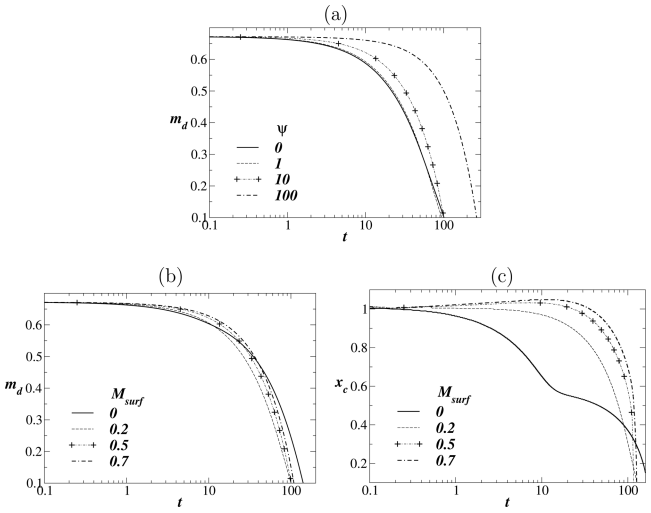

Figure 6. (a) Evolution of the drop mass for different values of ψ and $E = 0.005$. Evolution of (b) mass of the drop and (c) position of the contact line versus time for $\psi = 10$ and different values of M_{surf}. The rest of the parameter values are $E = 0.005$, $M_{par} = 0$, $\chi = 0$, and $\gamma = 0.1$.

decreases with increasing mass of the surfactant as shown in Figure 6b. To explain this behavior, it is necessary to investigate the effect of ψ on the spatiotemporal development of h, which is shown in Figure 7. For low values of ψ, the evaporative flux is

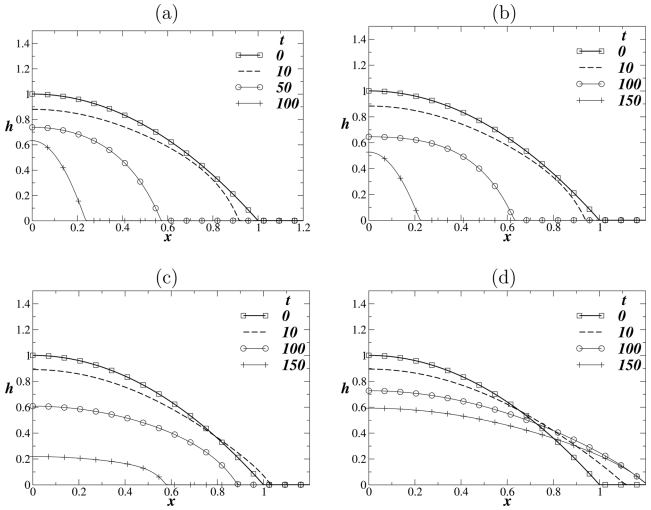

Figure 7. Evolution of the drop height, h, for (a) $\psi = 0$, (b) $\psi = 1$, (c) $\psi = 10$, and (d) $\psi = 100$. The rest of the parameter values are the same as those used to generate Figure 6b.

sufficiently strong so as to induce contact line recession during all stages of the evaporation process. With increasing ψ, however, J decreases leading to droplet evaporation accompanied by spreading; the degree of spreading is particularly pronounced for the largest values of ψ investigated and persists to advanced stages of the droplet dynamics (see Figure 6c). From eq 49, however, we see that the value of J near the apex is inversely proportional to the droplet thickness, h, which may explain the trends shown in Figure 6b. Because of the extensive spreading of the droplet, it retains a thinner profile for longer times. Regarding the flow field, we find that the formation of a recirculating vortex in the contact line region is delayed, whereas its size remains smaller throughout the simulation (see animation for Figure 7c in the Supporting Information, Movie S3).

3.2. Surfactant-Laden Droplets with Particles. We continue our study by taking into account the effect of noninteracting, surface-inactive particles in the droplet. Here, we consider finite values of the parameter ψ and therefore take into account the effect of surfactants on the evaporative flux, J. In Figure 8a,b, we show the spatiotemporal variation of the

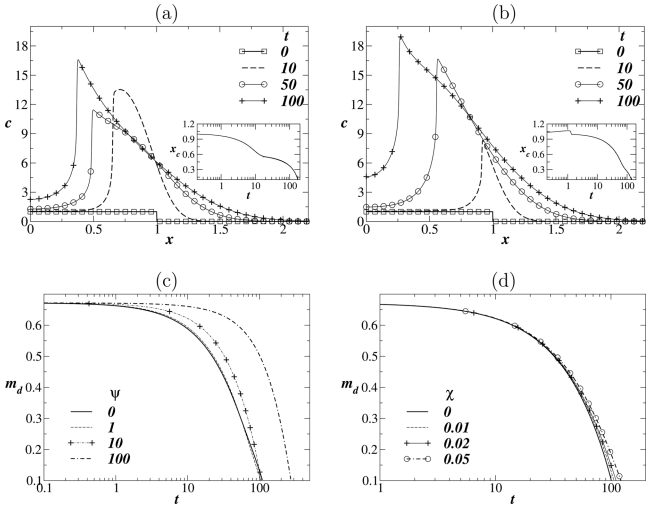

Figure 8. Evolution of particle concentration, c, profiles for (a) $M_{surf} = 0$ and (b) $M_{surf} = 0.5$ and $\psi = 10$; $\chi = 0.01$. Evolution of droplet mass for different values of (c) ψ for $\chi = 0.01$ and $M_{surf} = 0.5$ and (d) χ for $\psi = 10$ and $M_{surf} = 0.5$. The rest of the parameter values are $E = 0.005$, $M_{par} = 0.666$, and $\gamma = 0.1$. The insets in panels (a) and (b) show the temporal evolution of the contact line position.

particle concentration in the bulk in the presence and absence of the surfactant, respectively. It is seen that at early times c remains approximately constant over a large proportion of the drop before undergoing a rapid increase as the contact line region is approached, which is followed by a decay to zero in the precursor film region. The particle concentration becomes maximum in the contact line region because of the strong capillary flow there, which is responsible for the well-known coffee-stain effect.[10−12] In the surfactant-free case (see Figure 8a), the rapid retraction of the contact line because of the effect of thermal Marangoni stresses at intermediate times leads to a decrease of the maximum particle concentration as some particles are left behind; these particles eventually diffuse away from the droplet. At later stages, though, the contact line decelerates (see the insets of Figure 7a showing the temporal variation of x_c), resulting in the increase of particle concentration at the contact line; the deceleration of the contact line is also enhanced by the increasing viscosity due to the presence of particles (see eq 30). On the other hand, in the surfactant-laden case (see Figure 8b), the slower retraction of the contact line leads to a monotonic increase of the particle concentration in the contact line region. Regarding the droplet lifetime, as shown in Figure 8c, it does not appear to depend significantly on the presence of particles in the system. On the other hand, varying the value of the parameter ψ, we see the same trends in terms of evolution of the droplet mass, m_d as for the particle-free case (see Figure 8d). A typical evolution of the droplet profile along with the velocity field (x component) and the streamlines are shown in an animation in the Supporting

DOI: 10.1021/acs.langmuir.6b01042
Langmuir 2016, 32, 6871−6881

Information (Movie S4) for $E = 0.005$, $M_{surf} = 0.5$, $\psi = 10$, $M_{par} = 0.666$, $\chi = 0.01$, and $\gamma = 0.1$.

The final particle deposition patterns for the various cases under consideration can be evaluated by plotting in Figure 9a,b

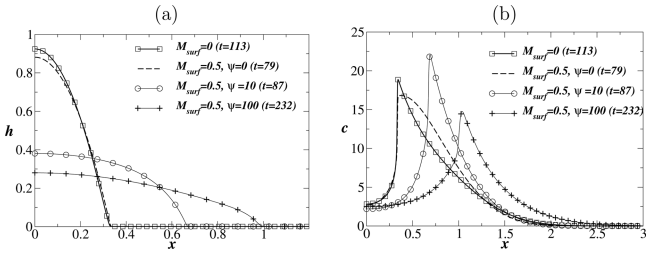

Figure 9. Profiles of the drop height, h, and particle concentration, c, at times for which m_d reaches 0.2. The rest of the parameter values are $E = 0.005$, $M_{par} = 0.666$, and $\chi = 0.01$.

the droplet shapes and particle concentration profiles, respectively, at times for which the droplet has lost 80% of its initial mass. Evidently, in the case of a particle-laden droplet, its shape at late stages of the evaporation process is significantly affected by the presence of surfactants and the value of the parameter, ψ, as it has already been established for a particle-free drop. Not surprisingly, the difference in the dynamics of evaporation because of the effect of surfactants is also reflected on the particle concentration profile, shown in Figure 9b. When we do not take into account the effect of the surfactant on the evaporative flux ($\psi = 0$), we find that the particle concentration profiles for the surfactant-free and the surfactant-laden cases are quite similar. The plateau that arises in the surfactant-laden case, in contrast to the sharp peak in the surfactant-free case, can be attributed to the somewhat slower retraction of the contact line. For finite values of ψ, though, the deposition patterns are markedly different because high values of ψ appear to promote contact line pinning and thus significantly enhance the coffee-stain effect.

To identify the physical mechanisms and how they affect the evaporation process of a particle-laden drop, we decomposed the average velocity in the bulk into its three main components (see eq 40), that is, the flow caused by the effect of capillary pressure, $\overline{u}_{ca}$, surfactant concentration gradients, $\overline{u}_{cg}$, and thermal gradients, $\overline{u}_{tg}$. As shown in Figure 10, the liquid is drawn toward the contact line because of the effect of capillary flow and surfactant concentration gradients and toward the droplet center because of the effect of thermal gradients. These results are clearly in agreement with the intuitive ideas and experimental findings presented by Hu and Larson.[15] We also see in Figure 10 that the capillary flow in the contact line region is enhanced in the case of a surfactant-free droplet or in the presence of surfactants for $\psi = 0$. Finite values of ψ result in the reduction of the effect of capillary flow, which is mostly due to the fact that the evaporative flux near the contact line decreases significantly because of the presence of surfactant molecules, and therefore, less liquid has to be drawn in the contact line region from the bulk. The decrease of the capillary flow also leads to less accumulation of the surfactant near the contact line, which results in smaller concentration gradients and thus a reduced effect of the solutal Marangoni stresses. Finally, with increasing value of ψ, the decrease of the evaporative flux also leads to a smaller variation of interfacial temperature, rendering the effect of thermal Marangoni stresses less pronounced.

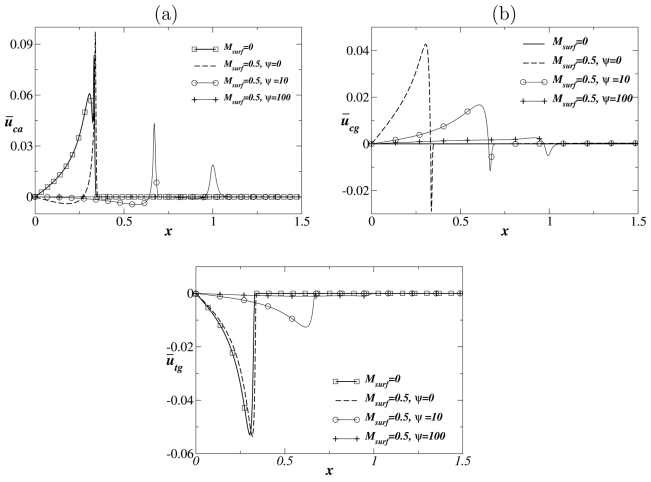

Figure 10. Profiles of $\overline{u}_{ca}$, $\overline{u}_{cg}$, and $\overline{u}_{tg}$ at times for which m_d reaches 0.2 for different values of M_{surf} and ψ. The rest of the parameter values are $\chi = 0.01$, $E = 0.005$, $M_{par} = 0.666$, and $\gamma = 0.1$.

4. CONCLUSIONS

We have studied the two-dimensional dynamics of a particle-laden volatile droplet on a superheated solid substrate in the presence of surfactants. Lubrication theory and rapid vertical diffusion of the surfactant and particles in the bulk are used in conjunction with asymptotic reduction to simplify the equations of heat, momentum, and mass conservation and derive a coupled system of evolution equations for the interface height, surfactant monomers, and bulk particle concentrations. The model accounts for the effect of solutal and thermal Marangoni stresses, interfacial and bulk diffusion of surfactant monomers and particles, respectively, as well as the effect of a varying viscosity depending on the local particle concentration. Crucially, our model also takes into account that surfactants may inhibit the evaporation rate by reducing the effective area along the liquid−air interface through which evaporation takes place.

We have used a finite-element formulation and an implicit Euler method in time to solve the system of evolution equations. A parametric study is carried out to investigate how the presence of surfactants affects the evaporation process as well as the flow dynamics with and without the presence of particles in the bulk. It is shown that the flow inside the evaporating droplet is driven by three different mechanisms, that is, the effect of capillary pressure and solutal and thermal Marangoni stresses, which also play a key role in the final particle deposition pattern. Moreover, the effect of surfactant monomers on the evaporative flux, through the reduction of the effective interfacial area through which evaporation is possible, affects significantly the action of these mechanisms especially near the contact line region. Our simulations indicate that when the effect of the surfactant on the evaporative flux is negligible, surfactant-laden, particle-free droplets evaporate more rapidly than their surfactant-free counterparts because of the suppression of the thermal Marangoni stresses-induced motion by the surfactant-driven Marangoni flow. Nevertheless, when the effect of the surfactant on the evaporative flux is appreciable, the evaporation process is retarded, leading to an increase of the droplet lifetime. We also show that for particle-laden droplets the particle deposition patterns are influenced strongly by the direct effect of the surfactant on the evaporative

DOI: 10.1021/acs.langmuir.6b01042
Langmuir 2016, 32, 6871−6881

flux; in certain cases, the coffee-stain effect is enhanced significantly.

■ ASSOCIATED CONTENT

Supporting Information

The Supporting Information is available free of charge on the ACS Publications website at DOI: 10.1021/acs.langmuir.6b01042.

Droplet profile along with the velocity field (x component) and the streamlines (AVI)
Droplet profile along with the velocity field (x component) and the streamlines (AVI)
Droplet profile along with the velocity field (x component) and the streamlines (AVI)
Droplet profile along with the velocity field (x component) and the streamlines (AVI)

■ AUTHOR INFORMATION

Corresponding Author

*E-mail: gkarapetsas@gmail.com.

Notes

The authors declare no competing financial interest.

■ ACKNOWLEDGMENTS

The authors wish to thank Professor Khellil Sefiane for very helpful discussions. O.K.M. acknowledges the support of the Engineering and Physical Sciences Research Council, U.K., through grant numbers EP/K003976 and EP/L020564.

■ REFERENCES

(1) Byun, M.; Laskowski, R. L.; He, M.; Qiu, F.; Jeffries-EL, M.; Lin, Z. Controlled Evaporative Self-Assembly of Hierarchically Structured Regioregular Conjugated Polymers. *Soft Matter* **2009**, *5*, 1583−1586.

(2) Chen, G.; Mohamed, G. J. Complex Protein Patterns Formation via Salt-Induced Self-Assembly and Droplet Evaporation. *Eur. Phys. J. E: Soft Matter Biol. Phys.* **2010**, *33*, 19−26.

(3) Han, W.; Lin, Z. Learning from "Coffee Rings": Ordered Structures Enabled by Controlled Evaporative Self-Assembly. *Angew. Chem., Int. Ed.* **2012**, *51*, 1534−1546.

(4) Sun, Y.; Xiao, G.; Lin, Y.; Su, Z.; Wang, Q. Self-Assembly of Large-Scale P3HT Patterns by Confined Evaporation in the Capillary Tube. *RSC Adv.* **2015**, *5*, 20491−20497.

(5) Blossey, R.; Bosio, A. Contact Line Deposits on cDNA Microarrays: A "Twin-Spot Effect". *Langmuir* **2002**, *18*, 2952−2954.

(6) Heim, T.; Preuss, S.; Gerstmayer, B.; Bosio, A.; Blossey, R. Deposition from a Drop: Morphologies of Unspecifically Bound DNA. *J. Phys.: Condens. Matter* **2005**, *17*, S703−S716.

(7) Sefiane, K. Patterns from Drying Drops. *Adv. Colloid Interface Sci.* **2014**, *206*, 372−381.

(8) Erbil, H. Y. Control of Stain Geometry by Drop Evaporation of Surfactant Containing Dispersions. *Adv. Colloid Interface Sci.* **2015**, *222*, 275−290.

(9) Larson, R. G. Transport and Deposition Patterns in Drying Sessile Droplets. *AIChE J.* **2014**, *60*, 1538−1571.

(10) Deegan, R. D.; Bakajin, O.; Dupont, T. F.; Huber, G.; Nagel, S. R.; Witten, T. A. Capillary Flow as the Cause of Ring Stains from Dried Liquid Drops. *Nature* **1997**, *389*, 827−829.

(11) Deegan, R. D.; Bakajin, O.; Dupont, T. F.; Huber, G.; Nagel, S. R.; Witten, T. A. Contact Line Deposits in an Evaporating Drop. *Phys. Rev. E* **2000**, *62*, 756−765.

(12) Deegan, R. D. Pattern Formation in Drying Drops. *Phys. Rev. E* **2000**, *61*, 475−485.

(13) Hu, H.; Larson, R. G. Analysis of the Effects of Marangoni Stresses on the Microflow in an Evaporating Sessile Droplet. *Langmuir* **2005**, *21*, 3972−3980.

(14) Hu, H.; Larson, R. G. Analysis of the Microfluid Flow in an Evaporating Sessile Droplet. *Langmuir* **2005**, *21*, 3963−3971.

(15) Hu, H.; Larson, R. G. Marangoni Effect Reverses Coffee-Ring Depositions. *J. Phys. Chem. B* **2006**, *110*, 7090−7094.

(16) Eral, H. B.; Augustine, D. M.; Duits, M. H. G.; Mugele, F. Suppressing the Coffee Stain Effect: How to Control Colloidal Self-Assembly in Evaporating Drops Using Electrowetting. *Soft Matter* **2011**, *7*, 4954−4958.

(17) Mampallil, D.; Eral, H. B.; van den Ende, D.; Mugele, F. Control of Evaporating Complex Fluids through Electrowetting. *Soft Matter* **2012**, *8*, 10614−10617.

(18) Orejon, D.; Sefiane, K.; Shanahan, M. E. R. Evaporation of Nanofluid Droplets with Applied DC Potential. *J. Colloid Interface Sci.* **2013**, *407*, 29−38.

(19) Wray, A. W.; Papageorgiou, D. T.; Craster, R. V.; Sefiane, K.; Matar, O. K. Electrostatic Suppression of the "Coffee Stain Effect". *Langmuir* **2014**, *30*, 5849−5858.

(20) Ristenpart, W. D.; Kim, P. G.; Domingues, C.; Wan, J.; Stone, H. A. Influence of Substrate Conductivity on Circulation Reversal in Evaporating Drops. *Phys. Rev. Lett.* **2007**, *99*, 234502.

(21) Truskett, V. N.; Stebe, K. J. Influence of Surfactants on an Evaporating Drop: Fluorescence Images and Particle Deposition Patterns. *Langmuir* **2003**, *19*, 8271−8279.

(22) Still, T.; Yunker, P. J.; Yodh, A. G. Surfactant-Induced Marangoni Eddies Alter the Coffee-Rings of Evaporating Colloidal Drops. *Langmuir* **2012**, *28*, 4984−4988.

(23) Semenov, S.; Trybala, A.; Agogo, H.; Kovalchuk, N.; Ortega, F.; Rubio, R. G.; Starov, V. M.; Velarde, M. G. Evaporation of Droplets of Surfactant Solutions. *Langmuir* **2013**, *29*, 10028−10036.

(24) Sempels, W.; De Dier, R.; Mizuno, H.; Hofkens, J.; Vermant, J. Auto-Production of Biosurfactants Reverses the Coffee Ring Effect in a Bacterial System. *Nat. Commun.* **2013**, *4*, 1757.

(25) Crivoi, A.; Duan, F. Amplifying and Attenuating the Coffee-Ring Effect in Drying Sessile Nanofluid Droplets. *Phys. Rev. E* **2013**, *87*, 042303.

(26) Crivoi, A.; Duan, F. Effect of Surfactant on the Drying Patterns of Graphite Nanofluid Droplets. *J. Phys. Chem. B* **2013**, *117*, 5932−5938.

(27) Marin, A.; Liepelt, R.; Rossi, M.; Kähler, C. J. Surfactant-Driven Flow Transitions in Evaporating Droplets. *Soft Matter* **2016**, *12*, 1593−1600.

(28) Morales, V. L.; Parlange, J.-Y.; Wu, M.; Pérez-Reche, F. J.; Zhang, W.; Sang, W.; Steenhuis, T. S. Surfactant-Mediated Control of Colloid Pattern Assembly and Attachment Strength in Evaporating Droplets. *Langmuir* **2013**, *29*, 1831−1840.

(29) Anyfantakis, M.; Geng, Z.; Morel, M.; Rudiuk, S.; Baigl, D. Modulation of the Coffee-Ring Effect in Particle/Surfactant Mixtures: The Importance of Particle-Interface Interactions. *Langmuir* **2015**, *31*, 4113−4120.

(30) Bhardwaj, R.; Fang, X.; Somasundaran, P.; Attinger, D. Self-Assembly of Colloidal Particles from Evaporating Droplets: Role of DLVO Interactions and Proposition of a Phase Diagram. *Langmuir* **2010**, *26*, 7833−7842.

(31) De Dier, R.; Sempels, W.; Hofkens, J.; Vermant, J. Thermocapillary Fingering in Surfactant-Laden Water Droplets. *Langmuir* **2014**, *30*, 13338−13344.

(32) Barnes, G. T. The Effects of Monolayers on the Evaporation of Liquids. *Adv. Colloid Interface Sci.* **1986**, *25*, 89−200.

(33) Lunkenheimer, K.; Zembala, M. Attempts to Study a Water Evaporation Retardation by Soluble Surfactants. *J. Colloid Interface Sci.* **1997**, *188*, 363−371.

(34) Barnes, G. T. The Potential for Monolayers to Reduce the Evaporation of Water from Large Water Storages. *Agric. Water Manage.* **2008**, *95*, 339−353.

(35) Davies, J. F.; Miles, R. E. H.; Haddrell, A. E.; Reid, J. P. Influence of Organic Films on the Evaporation and Condensation of Water in Aerosol. *Proc. Natl. Acad. Sci. U.S.A.* **2013**, *110*, 8807−8812.

DOI: 10.1021/acs.langmuir.6b01042
Langmuir 2016, 32, 6871−6881

(36) Hamzah, M. H.; Zain, S. M.; Khan, R. A.; Khalid, K. Study the Effect of Imposing Surfactants toward the Evaporation of Low Molecular Weight Alcohol. *Int. J. Environ. Sci. Dev.* **2013**, *4*, 403−407.
(37) Mikishev, A. B.; Nepomnyashchy, A. A. Instabilities in Evaporating Liquid Layer with Insoluble Surfactant. *Phys. Fluids* **2013**, *25*, 054109.
(38) Clay, M. A.; Miksis, M. J. Effects of Surfactant on Droplet Spreading. *Phys. Fluids* **2004**, *16*, 3070.
(39) Chan, K. Y.; Borhan, A. Surfactant-Assisted Spreading of a Liquid Drop on a Smooth Solid Surface. *J. Colloid Interface Sci.* **2005**, *287*, 233−248.
(40) Beacham, D. R.; Matar, O. K.; Craster, R. V. Surfactant-Enhanced Rapid Spreading of Drops on Solid Surfaces. *Langmuir* **2009**, *25*, 14174−14181.
(41) Karapetsas, G.; Craster, R. V.; Matar, O. K. On Surfactant-Enhanced Spreading and Superspreading of Liquid Drops on Solid Surfaces. *J. Fluid Mech.* **2011**, *670*, 5−37.
(42) Craster, R. V.; Matar, O. K.; Sefiane, K. Pinning, Retraction, and Terracing of Evaporating Droplets Containing Nanoparticles. *Langmuir* **2009**, *25*, 3601−3609.
(43) Kaplan, C. N.; Mahadevan, L. Evaporation-Driven Ring and Film Deposition From Colloidal Droplets. *J. Fluid Mech.* **2015**, *781*, R2-1−R2-13, DOI: 10.1017/jfm.2015.496.
(44) Burelbach, J. P.; Bankoff, S. G.; Davis, S. H. Nonlinear Stability of Evaporating/Condensing Liquid Films. *J. Fluid Mech.* **1988**, *195*, 463−494.
(45) Ajaev, V. S.; Homsy, G. M. Steady Vapor Bubbles in Rectangular Microchannels. *J. Colloid Interface Sci.* **2001**, *240*, 259−271.
(46) Ajaev, V. S. Spreading of Thin Volatile Liquid Droplets on Uniformly Heated Surfaces. *J. Fluid Mech.* **2005**, *528*, 279−296.
(47) Karapetsas, G.; Matar, O. K.; Valluri, P.; Sefiane, K. Convective Rolls and Hydrothermal Waves in Evaporating Sessile Drops. *Langmuir* **2012**, *28*, 11433−11439.
(48) Sultan, E.; Boudaoud, A.; Amar, M. B. Evaporation of a Thin Film: Diffusion of the Vapour and Marangoni Instabilities. *J. Fluid Mech.* **2005**, *543*, 183.
(49) Warner, M. R. E.; Craster, R. V.; Matar, O. K. Surface Patterning via Evaporation of Ultrathin Films Containing Nanoparticles. *J. Colloid Interface Sci.* **2003**, *267*, 92−110.
(50) Bligh, P. H.; Haywood, R. Latent Heat-Its Meaning and Measurement. *Eur. J. Phys.* **1986**, *7*, 245−251.
(51) Krieger, I. M. A Mechanism for Non-Newtonian Flow in Suspensions of Rigid Spheres. *J. Rheol.* **1959**, *3*, 137−152.
(52) Barnes, H. A. The Yield Stress—A Review or "*παντα ρει*"—Everything Flows? *J. Non-Newtonian Fluid Mech.* **1999**, *81*, 133−178.
(53) Kaplan, C. N.; Wu, N.; Mandre, S.; Aizenberg, J.; Mahadevan, L. Dynamics of evaporative colloidal patterning. *Phys. Fluids* **2015**, *27*, 092105.
(54) Wong, H.; Rumschitzki, D.; Maldarelli, C. On the Surfactant Mass Balance at a Deforming Fluid Interface. *Phys. Fluids* **1996**, *8*, 3203−3204.
(55) Pereira, A.; Kalliadasis, S. On the Transport Equation for an Interfacial Quantity. *Eur. Phys. J.: Appl. Phys.* **2008**, *44*, 211−214.
(56) Sheludko, A. Thin Liquid Films. *Adv. Colloid Interface Sci.* **1967**, *1*, 391−464.
(57) Gaver, D. P.; Grotberg, J. B. The Dynamics of a Localized Surfactant on a Thin Film. *J. Fluid Mech.* **1990**, *213*, 127−148.
(58) Moosman, S.; Homsy, G. M. Evaporating Menisci of Wetting Fluids. *J. Colloid Interface Sci.* **1980**, *73*, 212−223.
(59) Karapetsas, G.; Craster, R. V.; Matar, O. K. Surfactant-Driven Dynamics of Liquid Lenses. *Phys. Fluids* **2011**, *23*, 122106.
(60) Jensen, O. E.; Grotberg, J. B. The Spreading of Heat or Soluble Surfactant Along a Thin Liquid Film. *Phys. Fluids A* **1993**, *5*, 58−68.
(61) Bhardwaj, R.; Fang, X.; Attinger, D. Pattern Formation During the Evaporation of a Colloidal Nanoliter Drop: A Numerical and Experimental Study. *New J. Phys.* **2009**, *11*, 075020.

DOI: 10.1021/acs.langmuir.6b01042
Langmuir 2016, 32, 6871−6881